NIH Public Access
Author Manuscript
Magn Reson Med. Author manuscript; available in PMC 2013 April 1.

Published in final edited form as:
Magn Reson Med. 2012 April ; 67(4): 1159–1166. doi:10.1002/mrm.23077.

In Vivo Magnetic Resonance Imaging of Sodium and Diffusion in Rat Glioma at 21.1Tesla

Victor D. Schepkin[1], **Fabian Calixto Bejarano**[1], **Thomas Morgan**[2], **Shannon Gower-Winter**[2], **Manuel Ozambela Jr.**[2], and **Cathy W. Levenson**[2,3]

[1]National High Magnetic Field Laboratory, FSU, Tallahassee, FL

[2]Department of Biomedical Sciences, College of Medicine, FSU, Tallahassee, FL

[3]Program in Neuroscience, College of Medicine, FSU, Tallahassee, FL

Abstract

Sodium and diffusion MRI in intracranial rat 9L gliomas were evaluated over 6–8 days using the advanced sensitivity of sodium MRI at 21.1T. Glioma doubling time was 2.4–2.6 days. Glioma sodium signal was detected using the ultra-short echo time of 0.15 ms. The high resolution 3D sodium MRI with pixels of 0.125 μL allowed for minimizing a partial volume effect often relevant to the MRI of low intensity signals. Tumor sodium and diffusion MRI were evaluated for two separate sub-clones of 9L cells with different resistance to 1,3 bis(2-chloroethyl)-1-nitrosurea (BCNU) detected by pre-surgery assays. *In vivo*, after implantation, resistant 9L cells created tumors with significantly reduced sodium concentrations (57±3 mM) compared to non-resistant 9L cells (78±3 mM). The corresponding differences in diffusion were less, but also statistically significant. During tumor progression, an increase of glioma sodium concentration was observed in both cell types with a rate of 2.4–5.8 %/day relative to normal brain. Tumor diffusion was not significantly changed at this time, indicative of no alterations in glioma cellularity. Thus, changes in sodium during tumor progression reflect increasing intracellular sodium concentration and mounting metabolic stress. These experiments also demonstrate an enhanced sensitivity of sodium MRI to reflect tumor cell resistance.

Keywords

glioma resistance; sodium; diffusion; MRI; ultra high magnetic field

Introduction

Sodium MRI provides an independent window for *in vivo* processes taking place within tumors. While diffusion is gaining recognition as a tumor biomarker (1–4) the value of sodium MRI has yet to be established. The development of high field MRI scanners and short echo time imaging are the major advances allowing the difficulties relevant to sodium MR imaging to be overcome. Such progress makes sodium MRI both feasible and attractive as a method to investigate functional changes, especially in tumors (5–11). The recent imaging probe development allows for performing both sodium and water diffusion MRI of rats at the ultra high magnetic field of 21.1 T (12), thereby providing advanced capability for investigating the unique role of sodium homeostasis during cancer progression.

Address for correspondence: Victor D. Schepkin, Ph.D., Associate Scholar Scientist, Center for Interdisciplinary Magnetic Resonance, National High Magnetic Field Laboratory, 1800 East Paul Dirac Drive, Tallahassee, FL 32310, Tel: 850-645-7357, Fax: 850-644-1366, schepkin@magnet.fsu.edu, http://www.magnet.fsu.edu.

NIH-PA Author Manuscript
NIH-PA Author Manuscript
NIH-PA Author Manuscript

NIH-PA Author Manuscript

NIH-PA Author Manuscript

NIH-PA Author Manuscript

Sodium has great potential for the MRI of cancer. It is well known that a variety of ion movements are involved in the progression of apoptosis, a natural mechanism of cell self-elimination and a goal of many tumor therapies. Sodium, as part of this ion modulation and being visible through modern MRI, can convey valuable insights to apoptosis.

An increased sodium signal, often observed in gliomas (8,13–15), may be an indicator of the very early stages in mitochondrial malfunction and early signs of apoptosis. In contrast, maintenance of intracellular sodium concentrations may inhibit apoptosis (16–18). Further, sodium may serve as a marker of cell activity directed to augment tumor cell proliferation which can be accompanied by an excessive release of glutamate during glioma invasion (19,20).

Treatment of glioma, like many rapidly proliferating tumors, can be impaired by the development of drug resistance. In the present work we have examined the capability of *in vivo* sodium and diffusion MRI to reflect cellular alterations in resistivity and serve as a biomarker for drug resistance in the future.

Sodium alterations in untreated tumors have been previously detected (13,15,21–25). Weak sodium MR signals usually observed *in vivo* dictate selecting a low resolution matrix for sodium imaging. Consequently, for tumors either growing or shrinking, it is difficult to separate what part of the observed changes in the sodium signal are real and what part are due to a partial volume (PV) effect. At the low matrix size of 64 data points or less, the amount of pixels per tumor could be very low and the MR signal from the tumor could be significantly below the real values. For example, in the case of an acquisition matrix size of 64 and lesion size ~0.1 of field of view (FOV), the tumor itself will be represented by only 6 pixels. As a result, the MR intensity could be up to 38% below the maximum. It is important to note that this partial volume contribution will be changing non-linear during tumor growth or shrinking. Thus, advanced MR sensitivity, provided by high magnetic fields, is needed to overcome this problem. In the current study, high resolution sodium MRI with a pixel size of 0.125 μL and matrix of 128 data points was implemented. During data processing a three dimensional modeling of lesion size was used to correct the remaining partial volume effect.

The other important feature of sodium MRI is that sodium MR signals *in vivo* are heterogeneous and the free induction decay (FID) has a short time component of ~ 2 ms (26,27). The use of MRI with a large echo time of ~ 1 ms in previous experiments was not sufficient to detect a total sodium signal (23). A very short echo time of 0.15 ms and short readout (RO) time of 2.1 ms were used in the present study which allowed for detecting all sodium signals from the glioma.

The increased sensitivity to sodium achieved by using a record high magnetic field of 21.1 T (28) together with a very short echo and RO time for sodium detection provide the potential for an unbiased evaluation of sodium in glioma.

Methods

9L Glioma Cell Culture

Sub-cultures of rat 9L glioma cells were expanded in plastic flasks (75cm^2) with DMEM medium (Sigma Chemical Co., St Louis, MO), supplemented with 2 mM L-glutamine, 100 μg/mL gentamicin, 0.1% penicilline/streptomycin and 10% inactivated fetal bovine serum (complete medium). The cultures were incubated at 37°C in an atmosphere containing 5% CO_2. Immediately prior to implantation surgery, cells were harvested with 0.05% trypsin and 0.02% ethylenediaminetetraacetic acid (EDTA) and live cells counted using a

NIH-PA Author Manuscript

NIH-PA Author Manuscript

NIH-PA Author Manuscript

hemocytometer and trypan blue staining. Cells were then pelleted by centrifugation and re-suspended in pre-warmed serum free DMEM.

In vitro assay of 9L cell culture

Responsiveness of 9L cell sub-cultures *in vitro* to 1,3 bis(2-chloroethyl)-1-nitrosurea (BCNU) was determined using the *In Vitro* Toxicology Assay Kit (Sigma-Aldrich TOX-6) based on the sulforhodamine blue (SRB) method for monitoring cell viability. Briefly, 9L cells were plated in 96 well plates in triplicate at a density of 1×10^5 cells/ml and treated for 72 hours by BCNU using the range of concentrations from 0 μM to 150 μM. After 72 h, cells were fixed by adding 50 μL of ice cold 100% trichloroacetic acid per well for 1 h at 4° C. The plates were then rinsed, air dried and incubated with 100 μL of 0.4% sulforhodamine blue for 30 minutes. The plates were then washed with 1% acetic acid and air dried overnight. The incorporated dye was then solubilized with the addition of 200 μL of 10mM Tris buffer per well. Absorbance was read on a BioRad Benchmark Microplate reader at 490–530nm to characterize a concentration of protein. The results of tumor cell viability with different BCNU concentrations were fitted to an exponential function $y = m1 + m2*\exp(-c / m3)$. In this function "$y$" represents a concentration of 9L cells which was achieved after 72 h of incubation in the presence of BCNU given by concentration "c". In the plot a protein concentration without BCNU was normalized for 100%.

Intracranial Implantation of 9L Cells

All animal procedures have been approved by the Florida State University Animal Care and Use Committee (ACUC). Male Fisher rats weighing approximately 150 g were obtained from Charles River Laboratories (Wilmington, MA). Rats were anesthetized with isoflurane and fitted to a stereotaxic apparatus prior to receiving a 1 cm midline incision over the skull. A 1 mm burr hole was then made in the skull 2 mm anterior to bregma and 2.5 mm lateral to midline (right). This burr hole was used to deliver 100,000 9L resistant or non-resistant glioma cells in 10 μL serum free DMEM via a sterile Hamilton syringe to a depth of 3.5 mm. Following slow removal of the syringe, the burr hole was immediately sealed with bone wax and sutures (Prolene 5–0) were used to close the incision.

Magnetic Resonance Imaging

Eleven days after tumor implantation, animals were anesthetized with isoflurane and MRI experiments were conducted at the 21.1T MRI scanner using a double tuned radio-frequency (RF) probe with proton/sodium frequency = 900/237 MHz. Both proton and sodium coils comprised the volume coils and had a low pass bird cage design with ID of 33 mm and length of 55 mm. Animals were placed inside the RF coil using a solid bite bar, which was also used to deliver the anesthetic gas. The position of animal was adjusted to have the tumor at the center of the coil where the RF field is the most homogeneous. The temperature inside the magnet bore was controlled to 26° C and the animals were, additionally, covered by a thick paper blanket to facilitate animal temperature control while under anesthesia. Bruker Avance III console (PV 5.0 software) and gradient coils (RR Inc, ID = 64 mm) with GREAT60 amplifiers allowed gradients up to 0.6 T/m.

Sodium 3D back-projection MRI scans had a resolution of 0.5×0.5×0.5 mm, FOV = 64 mm and acquisition matrix of 128×180×90. The MRI pulse sequence was a modification of the ultra short echo time (UTE) 2D pulse sequence provided by Bruker Paravison software 5.0. The RO direction was rotated first in one plane using steps of 2° and 180 increments, and then the plane was rotated using the same steps of 2° and 90 increments. Spectral width for MRI was selected to be 30 KHz which permitted a minimum delay for sodium FID detection of ~ 0.15 ms and a short RO time of 2.1 ms. This sodium MRI setting permitted detection of virtually all sodium in the tumor, including bound intracellular sodium. Repetition time (TR)

NIH-PA Author Manuscript

NIH-PA Author Manuscript

NIH-PA Author Manuscript

=100 ms was chosen to minimize MR saturations of the *in vivo* sodium signals from the rodent brain having T_1 ~ 39 ms (28), and, as a result, the sodium scan time was 27 min.

The diffusion spin-echo (SE) pulse sequence had 3D diffusion gradients applied simultaneously in all 3 directions x, y, and z. Two "b" values were used for diffusion mapping of 100 and 1000 s/mm^2. The value "b" = 0 was avoided to minimize contributions from perfusion effects. Echo time (TE) was 34 ms and 15 slices were acquired with FOV of 30×30 mm and acquisition matrix of 128×128. Slice thickness (thk) was 0.7 mm and inter-slice distance was 1 mm. The repetition time for the diffusion scan of 3.75 s was selected to minimize saturation and slow transient changes in hardware. As a result, the duration of the diffusion MRI scan was 16 min.

Motion and flow compensation is a very important aspect for diffusion measurements. Special efforts were applied to reduce its effect. First, special shapes of diffusion gradients were selected to minimize flow artifacts (29,30). Second, a back-projection (BP) acquisition mode was implemented during diffusion MRI. In this case, the phase of each echo was used for additional motion/flow compensation by post processing.

Both sodium and diffusion MRI were performed on the same rat without repositioning the animal. This allowed for minimization of the total scan time and quality improvement of image co-registration. It also minimized the time between sodium and diffusion scans. The measurements of sodium and diffusion were presented in percent relative to a normal contra-lateral part of the brain, where the apparent diffusion coefficient (ADC) is ~ $0.78*10^{-3}$ mm^2/s (15) and sodium concentration is ~ 45 mM (13,31). The average tumor volume (*Tv*) values were non-linear fitted by function $Tv = a1*(2)^{time/a2}$, where a1 is initial tumor volume and a2 represents doubling time. The results of sodium concentration at all time points for all tumors were corrected for partial volume effect according to the growing tumor volume and procedure described in section "*Evaluation of Partial Volume Effect* " presented below. A base line correction was a part of image processing which was performed using Matlab 7.11 and Analyze 10. All errors were presented as a standard deviation (SD) of the mean from multiple slices for sodium and diffusion MRI.

Results

9L Cell In Vitro Characterization

9L cells have a natural capability for changes during cell handling. Two types of tumor 9L cells were selected for implantation having two different resistances to BCNU. The assays of these two sub-clones (Fig. 1) performed before cell implantation in animals show the difference of *in vitro* viability in the presence of increasing concentrations of BCNU. The differences for all data points are statistically significant ($p < 0.007$). The function $y = m1 + m2*\exp(-c / m3)$ was used to characterize the curves shown in Fig. 1 with fitting parameters and their errors presented in Table. 1. The naïve 9L sub-clone (the original type of 9L cells) had a 17.2% survival after 72 h of incubation with BCNU (n = 6), while the other sub-culture (derived from naïve) was significantly more resistant to BCNU (n = 3). There was also a large difference between these two cell lines in sensitivity at low concentrations of BCNU. Naïve cells displayed rapid population decay such that 19.1 μM of BCNU can decrease cell density 2.7 times, while for the resistant sub-culture it is necessary to have a BCNU concentration of 31.2 μM to reach the same effect (Table 1).

Magnetic Resonance Imaging

Examples of sodium MRI and proton diffusion maps of rat glioma can be seen in Fig. 2, which illustrates the images acquired using the current protocol for the implanted tumors and derived from the naïve sub-culture. The images show the tumor as areas with sharply

NIH-PA Author Manuscript

NIH-PA Author Manuscript

NIH-PA Author Manuscript

elevated sodium intensity or increased diffusion relative to a normal rat brain. The region of the tumor on the sodium image and diffusion map was selected automatically by Analyze software on the level of 0.6 of the difference between the tumor values and the surrounding normal brain. The increased ADC values at the low part of brain are the result of non-ideal local motion compensation in that part of the brain.

Results of the sodium and diffusion *in vivo* MRI for both types of 9L cells at 11 days after tumor implantation, are presented in Fig. 3 (n = 5 for each group). The tumor created by naïve 9L cells had a sodium concentration of 173.4 ± 6.5% (SD) relative to the normal brain, while the resistant group had a sodium concentration of only 126.7 ± 7.5% (SD) ($p < 0.001$). The values of sodium concentration were corrected for partial volume effect. Diffusion values in both tumors were also statistically different ($p = 0.012$). The tumor produced from naïve 9L cells had a diffusion of 150.9 ± 5.7% (SD) relative to the normal brain while tumors derived from resistant 9L cells had the corresponding value of 140.1 ± 4.8% (SD).

The time course of the tumor sodium concentration and diffusion for tumors formed by the naïve group of 9L cells is given in Fig. 4 (n = 3). The time scale on the figure was given from tumor implantation. It is noticeable that the sodium concentration in the tumor was steadily increasing over time. The fit of changes by linear function yielded a rate of increase of 2.4 ± 0.6% (SD) per day ($R^2 = 0.964$). The contra-lateral area (normal brain) was determined for each slice representing the tumor. It was a freehand area approximately matching the tumor size or less according to the available brain space on the slice. There were practically no changes in diffusion at the same time. The linear function fit gives the rate of only 1.4 ± 0.5% (SD) per day ($R^2 = 0.867$).

The corresponding time course of tumor sodium concentration and diffusion from the resistant glioma cells is given in Fig. 5. Again, there is almost no change in diffusion; the fit by linear function of the changes in tumor diffusion gives a rate of 1.2 ± 0.8% (SD) per day ($R^2 = 0.715$). The corresponding linear fit of sodium concentration in the tumor gives a rate of increase of 5.8 ± 0.8% (SD) per day ($R^2 = 0.986$). A minor but non-significant increase of sodium concentration in contra-lateral brain was seen at this time while there were no corresponding changes in diffusion here.

In a few cases both sodium and diffusion images revealed a development of necrosis in the tumor interior after day 18 post-implantation. Within these necrotic areas, a 300% increase in total sodium was observed. In addition, diffusion at the same place was also increased to 230% relative to the normal contra-lateral brain.

Evaluation of Partial Volume Effect

The contribution of the partial volume effect is relevant to any MRI with low resolution. The drop in intensity is almost always present during imaging of the weak MR signals. In this case, due to the low sensitivity, very often a small acquisition matrix is selected down to 32×32×32. Additionally, this eventually leads to a low number of pixels covering the lesion. As a result a decreased MR signal intensity is usually detected from the lesion relative to the surrounding areas. Most importantly, the level of these changes is dependent on the size of the tumor lesion. In the present study, the time courses of tumor volumes are presented in Fig. 6. The results give the range of changes for both 9L cell lines for the time frame starting on day 11 after surgery. The non-linear fit of tumor volume changes to a model function (see Methods) gives the doubling time of 2.4 ± 0.2 (SD) days ($R^2 = 0.995$) for the tumors from naïve cells and of 2.6 ± 0.1 (SD) days ($R^2 = 0.999$) for the tumors from the resistant cell line.

NIH-PA Author Manuscript

NIH-PA Author Manuscript

NIH-PA Author Manuscript

The current experiments were performed with the k space matrix of np = 128. Such imaging dimension increases amount of pixels for the lesion and minimizes the PV effect but it is still present (Fig. 7). The 3D modeling was performed in Matlab to evaluate this remaining partial volume effect in our experiments. The lesion was modeled by sphere with the diameter changing from 1 mm to 64 mm or to the size of FOV. The reference for 100% was obtained using the maximum spherical lesion size inside the k-space of 128×128×128.

Additional contribution to PV effect may occur due to the decay of the FID during RO time. For evaluation of this effect a reasonable bi-exponential function was selected to represent sodium MR signal decay: $F = p1*\exp(-n / (SW*T_{2a})) + p2*\exp(-n / (SW*T_{2b})$. Here, $p1 = 0.3$ and $p2 = 0.7$ represent relative amplitudes of the fast and slow components of the FID, $1/SW$ is time increment during FID acquisition (in our case it was 33 μs), n is a current number of the FID point, the relaxation parameters were $T_{2a} = 2$ ms and $T_{2b} = 15$ ms. The decay function F was applied along each RO direction in k-space, the results later were re-gridded in Matlab before FT processing. The effect of bi-exponential FID is presented on Fig. 7 by the dotted line.

It is important to keep in mind, that the partial volume effect corrections need to be applied to the difference in intensity between lesion and the surrounding areas. A contribution from the partial volume effect is more noticeable for small lesions. A four time increase of lesion volume from V = 17 μL (diameter = 3.2 mm) up to V = 100 μL (diameter =5.8 mm) will have PV corrections range from 60% to 80% (Fig. 7). Note that all values are below 100% which can be important for absolute quantifications. Correction values applied to the tumor intensity relative to the surrounding area will give the rate of sodium concentration increase of 2.4 ± 0.6% (SD) per day. Without corrections this rate would have been 4.3 ± 0.6% (SD) per day. For the resistant cell the tumor volume was changing from V = 100 μL (diameter = 5.8 mm) to 380 μL (diameter = 9 mm), the PV effect will be changed from 80% to 88%. A larger tumor volume and a smaller difference of tumor sodium concentration relative to surrounding areas both were affecting the results of corrections. The corrected rate of sodium concentration increase is 5.8 ± 0.8% (SD) per day, without corrections it would have been only 5.7 ± 0.7% per day.

The above corrections were performed for an acquisition matrix of 128×128×128. However, for a smaller amount of voxels per lesion volume, the partial volume effect could be much more pronounced. The non-linear contributions of the partial volume effect relevant to the tumor size were corrected separately for each time point of tumor growth. Due to the assumptions in selecting of the bi-exponential function, the additional corrections for the possible bi-exponential FID were not applied, but its effect was incorporated into the model for illustration.

Discussion

The present study demonstrates differences between sodium and diffusion MRI in rat 9L glioma cells implanted intra-cranially and imaged *in vivo*. It is difficult to accept without reservations that the increased diffusion and sodium contents in tumors are due solely to the micro-structural changes and increased extracellular space. The results demonstrate that changes in glioma sodium and diffusion can be independent, and thus could have different origins. A confirmation of independence between sodium and diffusion in tumors can be seen in the values of diffusion and sodium in subcutaneous tumors. For example, diffusion in subcutaneous 9L tumors (32) is much less than in the surrounding normal areas; while in glioma, the diffusion is usually above the values of a normal brain. However, sodium concentration in a tumor is usually above the normal values of nearby tissue for both

NIH-PA Author Manuscript

NIH-PA Author Manuscript

NIH-PA Author Manuscript

subcutaneous and intracranial tumors. Thus, it is becoming more apparent that sodium reflects changes in tumor cells beyond the possible variations of their extracellular spaces.

The types of 9L cells used in the present study have different BCNU response profiles in the SRB assay even though these cells had a limited passage number and neither was subjected to any chemotherapeutic challenges. This is not surprising as it has already been shown that cultures with multiple passages can be distinct from the original tumor (33,34). Consistent with these reports, our earlier unpublished observations have shown that changes associated with increased passage number in 9L cells have a dramatic impact on MRI results such that high passage cells *in vivo* yield a dramatically decreased sodium concentration and diffusion in tumor tissue compared to the low passage tumors. However, there is no linear dependence on the number of passages. This study gives an example of cell alterations which could be observed even for low passage cancer cells and the capability to detect such changes with SRB assays and MRI.

In response to this situation, it is our practice to work with a cell passage number below 5 and to characterize the cells based on their viability in the presence of increasing concentrations of BCNU immediately prior to intracranial implantation.

The very important observation in this study is that two groups of 9L cells with different resistance to BCNU *in vitro* create two different types of tumors. The difference between them was not only detected but statistically significant for both sodium ($p < 0.001$) and diffusion ($p < 0.012$) MRI. The observed difference is especially dramatic for sodium MRI. Sodium concentration in naïve glioma was 78 ± 3 mM and for resistant glioma it was 57 ± 3 mM. With tumor progression tumor sodium concentration was increasing with a constant rate and showed no dependence on tumor size. Both tumors were growing at this time and their volumes increased more than three times. The doubling time of 2.6 days for the tumor from naïve 9L cells and 2.4 days for the tumor from resistant type cells found in this study are comparable with the results of others (35).

Unchanging diffusion during 9L rodent glioma growth suggests that there are no structural variations in tumor cellularity. Thus, the observed increase of sodium within a tumor is a result of intracellular sodium increase in tumor cells. It can be assumed that tumor intracellular volume is 75% of the total and remains static. Thus, for the normal brain sodium content of ~ 45 mM, the observed ~ 5.8% increase of sodium signal in glioma represents an intracellular sodium increase in the tumor of ~ 3.4 mM/day. It is much more than the value observed earlier of 1.6 mM/day (15). However, the previous data was acquired with a large echo time of ~ 0.5 ms, thus it was not a total sodium signal and the low size acquisition matrix of 32×32×32 could have a large contribution from the partial volume effect. The observed rising of intracellular sodium concentration in glioma cells tends to take place once the tumor starts growing.

While an increase in blood supply to the tumor may contribute to the sodium content in the tumor, it is usually small (36). From estimation a 50% increase of glioma sodium concentration relative to normal brain would require an increase of blood vessel volume ~ 16%, which is far above the few percentage points expected due to an increase in the blood vessel growth.

Many cancer cells have a deficit of adenosine triphosphate (ATP) production (37). This could be one of the reasons that tumors have an increased sodium concentration. Lactate overproduction is an indicator of increased glycolysis in tumors even during aerobic conditions. It is also a sign of the decreased production of ATP which is needed for the Na/K pump function and active synthesis inside the cell for ongoing cell division. As a result, intracellular sodium may be increasing due to a deficit of ATP. As lactate production tends

NIH-PA Author Manuscript

NIH-PA Author Manuscript

NIH-PA Author Manuscript

to correlate with tumor aggressiveness (38), the increasing intracellular sodium content could be an indicator of growing tumor malignancy. This point of view is supported by X-ray analysis, where an increase in tumor sodium was correlated with tumor malignancy (39,40). Increased sodium content was also detected in many other tumors and changes in Na/K ATPase activity may account for these alterations (18).

There are multiple reports suggesting that the level of ATP can decrease with tumor progression (21,22,41,42). The observed steady increase of tumor sodium concentration during tumor growth can be a reflection of a changing level in the ATP supply. It is also known that during tumor growth, pH and other metabolic stresses mount (38), and an increase in glioma sodium concentration could indicate changes which eventually lead to tumor necrosis.

It appears that some cancer cells may compensate for the ATP deficit by having more efficient mitochondria and, consequently, the tumor sodium concentration can have decreased values. The present experiments show a correlation of such changes with an increase in the resistance of cancer cells. New experiments are in progress to investigate this possibility with more detail.

Conclusion

The results of this study demonstrate that the initial sodium concentration in the tumor could convey important information about the level of drug resistance before tumor therapy. Observation of the tumor sodium concentration indicates that sodium MRI is more sensitive than diffusion in detecting the small modulation in tumor cell resistance. Thus, in practice, sodium MRI contrast of tumors could be a sensitive marker of minor changes in tumor cell resistance. The progression of glioma was accompanied by a steady increase in tumor sodium concentration, revealing an increase of tumor intracellular sodium taking place apparently from the time of tumor implantation. The observed changes of sodium concentration may reflect alterations of tumor cells during growth and the increasing metabolic stress leading to malignancy. The partial volume effect relevant to MRI of low intensity signals was evaluated and dramatically reduced by modeling and utilizing the advanced sodium MRI sensitivity of the high field of 21.1 T. Sodium and diffusion MRI at 21.1 T are capable of providing accurate results for a single animal and present a unique opportunity for detection and investigation of tumor resistance.

Acknowledgments

Special thanks to P. Gor'kov, C. Qian, B. Beck, W. Brey, S. Grant and R. Desilets for the double tuned RF probe development. The authors are grateful to Silvia M. Figueiroa, Ashley K. Blue, Nathaniel Falconer, and Kiran K. Shetty for their valuable support. Many thanks to Prof. Thomas L. Chenevert, Prof. Brain D. Ross, Prof. Alnawaz Rehemtulla (University of Michigan), Prof. Tim Cross, and Prof. Greg Boebinger (NHMFL/FSU) for their invaluable help in the initial steps of this project. The *in vivo* rodent studies were supported by NIH Grant R21 CA119177. This work was supported by National Science Foundation Cooperative Agreement No. DMR-0654118, the State of Florida, and the U.S. Department of Energy.

References

1. Arlinghaus LR, Li X, Levy M, Smith D, Welch EB, Gore JC, Yankeelov TE. Current and future trends in magnetic resonance imaging assessments of the response of breast tumors to neoadjuvant chemotherapy. Journal of oncology. 2010:2010.
2. Chenevert TL, Ross BD. Diffusion imaging for therapy response assessment of brain tumor. Neuroimaging clinics of North America. 2009; 19(4):559–571. [PubMed: 19959005]
3. Tsien C, Galban CJ, Chenevert TL, Johnson TD, Hamstra DA, Sundgren PC, Junck L, Meyer CR, Rehemtulla A, Lawrence T, Ross BD. Parametric response map as an imaging biomarker to

NIH-PA Author Manuscript

NIH-PA Author Manuscript

NIH-PA Author Manuscript

distinguish progression from pseudoprogression in high-grade glioma. J Clin Oncol. 2010; 28(13): 2293–2299. [PubMed: 20368564]

4. Thoeny HC, Ross BD. Predicting and monitoring cancer treatment response with diffusion-weighted MRI. J Magn Reson Imaging. 2010; 32(1):2–16. [PubMed: 20575076]
5. Jacobs MA, Stearns V, Wolff AC, Macura K, Argani P, Khouri N, Tsangaris T, Barker PB, Davidson NE, Bhujwalla ZM, Bluemke DA, Ouwerkerk R. Multiparametric magnetic resonance imaging, spectroscopy and multinuclear ((2)(3)Na) imaging monitoring of preoperative chemotherapy for locally advanced breast cancer. Academic radiology. 2010; 17(12):1477–1485. [PubMed: 20863721]
6. Ouwerkerk R, Jacobs MA, Macura KJ, Wolff AC, Stearns V, Mezban SD, Khouri NF, Bluemke DA, Bottomley PA. Elevated tissue sodium concentration in malignant breast lesions detected with non-invasive 23Na MRI. Breast cancer research and treatment. 2007; 106(2):151–160. [PubMed: 17260093]
7. Thulborn KR, Lu A, Atkinson IC, Damen F, Villano JL. Quantitative sodium MR imaging and sodium bioscales for the management of brain tumors. Neuroimaging clinics of North America. 2009; 19(4):615–624. [PubMed: 19959008]
8. Kline RP, Wu EX, Petrylak DP, Szabolcs M, Alderson PO, Weisfeldt ML, Cannon P, Katz J. Rapid in vivo monitoring of chemotherapeutic response using weighted sodium magnetic resonance imaging. Clin Cancer Res. 2000; 6(6):2146–2156. [PubMed: 10873063]
9. Atkinson IC, Sonstegaard R, Pliskin NH, Thulborn KR. Vital signs and cognitive function are not affected by 23-sodium and 17-oxygen magnetic resonance imaging of the human brain at 9.4 T. J Magn Reson Imaging. 2010; 32(1):82–87. [PubMed: 20578014]
10. Boada FE, Tanase C, Davis D, Walter K, Torres-Trejo A, Couce M, Hamilton R, Kondziolka D, Bartynski W, Lieberman F. Non-invasive assessment of tumor proliferation using triple quantum filtered 23/Na MRI: technical challenges and solutions. Conf Proc IEEE Eng Med Biol Soc. 2004; 7:5238–5241. [PubMed: 17271521]
11. Babsky AM, Hekmatyar SK, Zhang H, Solomon JL, Bansal N. Application of 23Na MRI to monitor chemotherapeutic response in RIF-1 tumors. Neoplasia. 2005; 7(7):658–666. [PubMed: 16026645]
12. Gor'kov, PL.; Qian, C.; Beck, BL.; Clark, M.; Masad, IS.; Schepkin, VD.; Grant, SC.; Brey, WW. A modular MRI probe for large rodent neuroimaging at 21.1 T (900 MHz). Proceeding, 17th Annual Meeting, ISMRM; Honolulu, Hawai'i, USA. 2009. p. 2952
13. Thulborn KR, Davis D, Adams H, Gindin T, Zhou J. Quantitative tissue sodium concentration mapping of the growth of focal cerebral tumors with sodium magnetic resonance imaging. Magn Reson Med. 1999; 41(2):351–359. [PubMed: 10080284]
14. Ouwerkerk R, Bleich KB, Gillen JS, Pomper MG, Bottomley PA. Tissue sodium concentration in human brain tumors as measured with 23Na MR imaging. Radiology. 2003; 227(2):529–537. [PubMed: 12663825]
15. Schepkin VD, Ross BD, Chenevert TL, Rehemtulla A, Sharma S, Kumar M, Stojanovska J. Sodium magnetic resonance imaging of chemotherapeutic response in a rat glioma. Magn Reson Med. 2005; 53(1):85–92. [PubMed: 15690506]
16. Bortner CD, Cidlowski JA. Uncoupling cell shrinkage from apoptosis reveals that Na+ influx is required for volume loss during programmed cell death. J Biol Chem. 2003; 278(40):39176–39184. [PubMed: 12821680]
17. Bortner CD, Cidlowski JA. Cell shrinkage and monovalent cation fluxes: role in apoptosis. Arch Biochem Biophys. 2007; 462(2):176–188. [PubMed: 17321483]
18. Chen JQ, Contreras RG, Wang R, Fernandez SV, Shoshani L, Russo IH, Cereijido M, Russo J. Sodium/potassium ATPase (Na+, K+-ATPase) and ouabain/related cardiac glycosides: A new paradigm for development of anti- breast cancer drugs? Breast cancer research and treatment. 2006; 96(1):1–15. [PubMed: 16322895]
19. Sontheimer H. Malignant gliomas: perverting glutamate and ion homeostasis for selective advantage. Trends Neurosci. 2003; 26(10):543–549. [PubMed: 14522147]
20. Sontheimer H. A role for glutamate in growth and invasion of primary brain tumors. J Neurochem. 2008; 105(2):287–295. [PubMed: 18284616]

NIH-PA Author Manuscript

NIH-PA Author Manuscript

NIH-PA Author Manuscript

21. Stubbs M, Veech RL, Griffiths JR. Tumor metabolism: the lessons of magnetic resonance spectroscopy. Advances in enzyme regulation. 1995; 35:101–115. [PubMed: 7572338]
22. Winter PM, Poptani H, Bansal N. Effects of chemotherapy by 1,3-bis(2-chloroethyl)-1-nitrosourea on single-quantum- and triple-quantum-filtered 23Na and 31P nuclear magnetic resonance of the subcutaneously implanted 9L glioma. Cancer research. 2001; 61(5):2002–2007. [PubMed: 11280759]
23. Schepkin, VD. Sodium MRI clocks pre-necrotic alterations in rat glioma without changes in tumor diffusion. Proceedings of The Joint Annual Meetiing ISMRM-ESMRMB; May 19–25, 2007; Berlin, Germany. 2007. p. 2997
24. Babsky, AM.; Ju, S.; Bennett, S.; Atthe, B.; George, B.; McLennan, G.; Bansal, N. Proceeding of the 17th Annual Meeting of ISMRM; 2009. p. 4153
25. Babsky AM, Zhang H, Hekmatyar SK, Hutchins GD, Bansal N. Monitoring chemotherapeutic response in RIF-1 tumors by single-quantum and triple-quantum-filtered (23)Na MRI, (1)H diffusion-weighted MRI and PET imaging. Magnetic resonance imaging. 2007; 25(7):1015–1023. [PubMed: 17707164]
26. Rooney WD, Springer CS Jr. The molecular environment of intracellular sodium: 23Na NMR relaxation. NMR in biomedicine. 1991; 4(5):227–245. [PubMed: 1751346]
27. Boada FE, Christensen JD, Huang-Hellinger FR, Reese TG, Thulborn KR. Quantitative in vivo tissue sodium concentration maps: the effects of biexponential relaxation. Magn Reson Med. 1994; 32(2):219–223. [PubMed: 7968444]
28. Schepkin VD, Brey WW, Gor'kov PL, Grant SC. Initial in vivo rodent sodium and proton MR imaging at 21.1 T. Magnetic resonance imaging. 2010; 28(3):400–407. [PubMed: 20045599]
29. Wong EC, Cox RW, Song AW. Optimized isotropic diffusion weighting. Magn Reson Med. 1995; 34(2):139–143. [PubMed: 7476070]
30. Chenevert TL, McKeever PE, Ross BD. Monitoring early response of experimental brain tumors to therapy using diffusion magnetic resonance imaging. Clin Cancer Res. 1997; 3(9):1457–1466. [PubMed: 9815831]
31. Christensen JD, Barrere BJ, Boada FE, Vevea JM, Thulborn KR. Quantitative tissue sodium concentration mapping of normal rat brain. Magn Reson Med. 1996; 36(1):83–89. [PubMed: 8795025]
32. Schepkin VD, Lee KC, Kuszpit K, Muthuswami M, Johnson TD, Chenevert TL, Rehemtulla A, Ross BD. Proton and sodium MRI assessment of emerging tumor chemotherapeutic resistance. NMR in biomedicine. 2006; 19(8):1035–1042. [PubMed: 16894643]
33. Yung WK. In vitro chemosensitivity testing and its clinical application in human gliomas. Neurosurgical review. 1989; 12(3):197–203. [PubMed: 2682352]
34. Izumu I, Mineura K, Watanabe K, Kowada M. Characterization and chemosensitivity of two cell lines derived from human glioblastomas. Journal of neuro-oncology. 1993; 17(2):111–121. [PubMed: 8145054]
35. Kim B, Chenevert TL, Ross BD. Growth kinetics and treatment response of the intracerebral rat 9L brain tumor model: a quantitative in vivo study using magnetic resonance imaging. Clin Cancer Res. 1995; 1(6):643–650. [PubMed: 9816027]
36. Pathak AP, Penet MF, Bhujwalla ZM. MR molecular imaging of tumor vasculature and vascular targets. Advances in genetics. 2010; 69:1–30. [PubMed: 20807600]
37. Solaini G, Sgarbi G, Baracca A. Oxidative phosphorylation in cancer cells. Biochimica et biophysica acta. 2010
38. McCarty MF, Whitaker J. Manipulating tumor acidification as a cancer treatment strategy. Altern Med Rev. 2010; 15(3):264–272. [PubMed: 21155627]
39. Nagy I, Lustyik G, Lukacs G, Nagy V, Balazs G. Correlation of malignancy with the intracellular Na+:K+ ratio in human thyroid tumors. Cancer research. 1983; 43(11):5395–5402. [PubMed: 6616471]
40. Cameron I, Hunter K. An x-ray-microanalysis study on the progressive increase in intracellular sodium concentration associated with DMH induction of colon cancer. Proceeding of the American Association for Cancer Research. 1984 March 25.:131.

NIH-PA Author Manuscript

NIH-PA Author Manuscript

NIH-PA Author Manuscript

41. Steen RG, Tamargo RJ, Brem H, Glickson JD, Wehrle JP. In vivo 31P nuclear magnetic resonance spectroscopy of rat 9L gliosarcoma treated with BCNU: dose response of spectral changes. Magn Reson Med. 1989; 11(2):258–266. [PubMed: 2779416]

42. Steen RG, Tamargo RJ, McGovern KA, Rajan SS, Brem H, Wehrle JP, Glickson JD. In vivo 31P nuclear magnetic resonance spectroscopy of subcutaneous 9L gliosarcoma: effects of tumor growth and treatment with 1,3-bis(2-chloroethyl)-1-nitrosourea on tumor bioenergetics and histology. Cancer research. 1988; 48(3):676–681. [PubMed: 3335030]

NIH-PA Author Manuscript
NIH-PA Author Manuscript
NIH-PA Author Manuscript

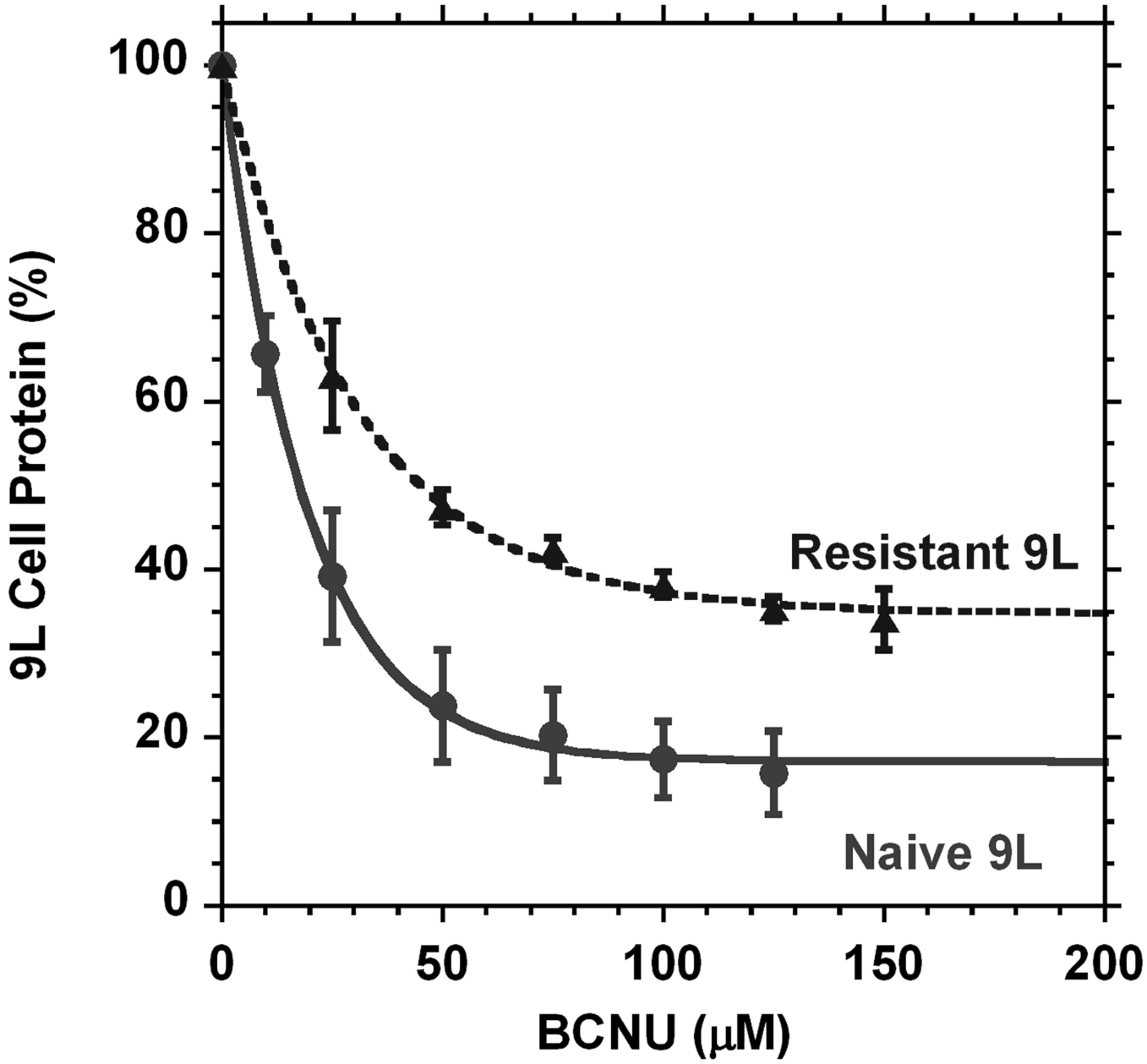

Fig. 1.

In vitro assays for two types of low passage 9L cells selected for implantation. The amount of cells capable of surviving 72 hour cultivation in BCNU containing media decreases with an increase of BCNU concentration. Naïve type (●, n = 3) 9L cells are more sensitive to the chemo-therapeutic agent concentration than their resistant counterpart (▲, n = 6). The differences for all data points are statistically significant ($p < 0.007$). Error bars represent standard deviations. The amount of cells at the beginning of cultivation was normalized to 100%.

NIH-PA Author Manuscript
NIH-PA Author Manuscript
NIH-PA Author Manuscript

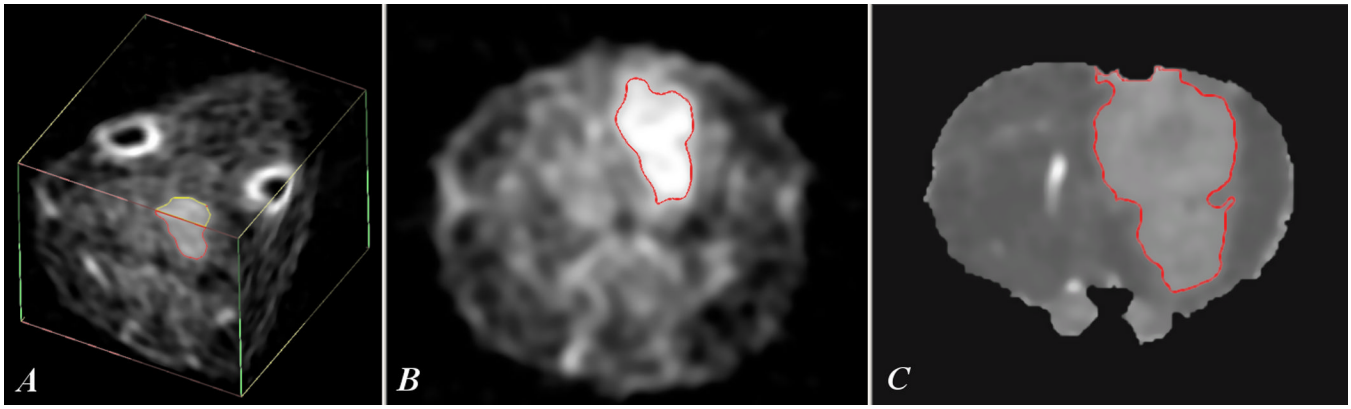

Fig. 2.

Sodium MRI and diffusion map of 9L glioma at day 17 after tumor implantation. Sodium 3D image (A) shows the location of the tumor and a position of slices through the center of tumor used for images (B) and (C). Image (B) illustrates a tumor selection for sodium MRI (slice thk = 1 mm), image (C) represents a corresponding tumor selection for the diffusion map (slice thk = 0.7 mm). The slice position on images (B) and (C) was ~ 9 mm relative to the back of the brain.

NIH-PA Author Manuscript
NIH-PA Author Manuscript
NIH-PA Author Manuscript

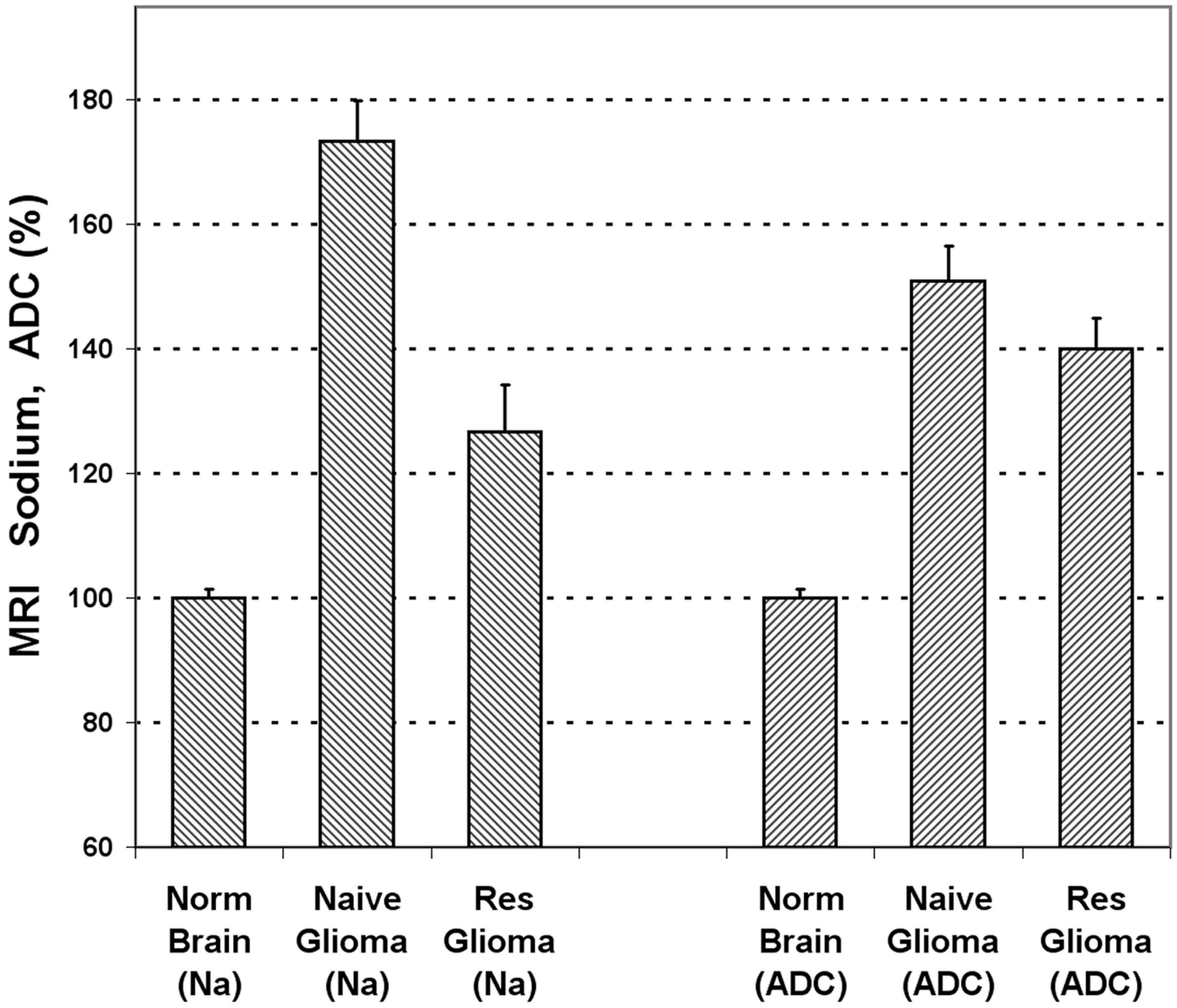

Fig. 3.

In vivo sodium and diffusion MRI of two rat gliomas at 11 days after 9L cell implantation. The values of sodium and diffusion are given in percent relative to the contra-lateral normal brain. Error bars represent standard deviations. The difference between tumors created by naïve and resistant cell lines are statistically significant for both sodium concentration ($n = 5$, $p = 0.0003$) and diffusion ($n = 5$, $p = 0.012$). It is important to note that sodium MRI is more sensitive to changes in glioma resistance.

NIH-PA Author Manuscript
NIH-PA Author Manuscript
NIH-PA Author Manuscript

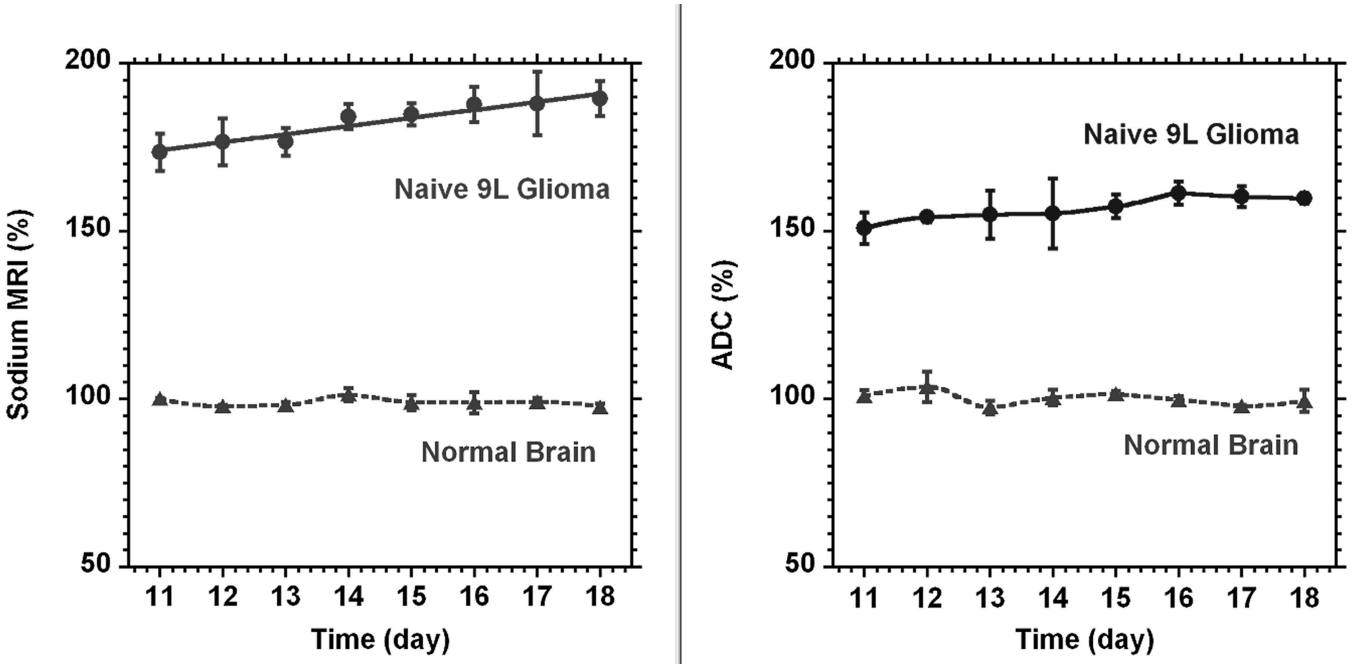

Fig. 4.

The time courses of sodium (left) and diffusion (right) MRI for a naïve type 9L glioma (●, n = 3). The time scale on the figure was given from tumor implantation. Sodium and diffusion MRI data are given in percent relative to normal contra-lateral brain (▲). The data for tumor sodium concentration were fitted by a linear function. The reference (100%) was the average of all sodium or diffusion data through the time course. All data points are presented as mean ± SD. Sodium concentration in the tumor steadily increased with the rate 2.4 ± 0.6% (SD) per day. Diffusion was practically unchanged (1.4 ± 0.5% (SD) per day). Sodium values were corrected for partial volume effect. Curves for normal brain and diffusion in glioma were created by smooth function.

NIH-PA Author Manuscript
NIH-PA Author Manuscript
NIH-PA Author Manuscript

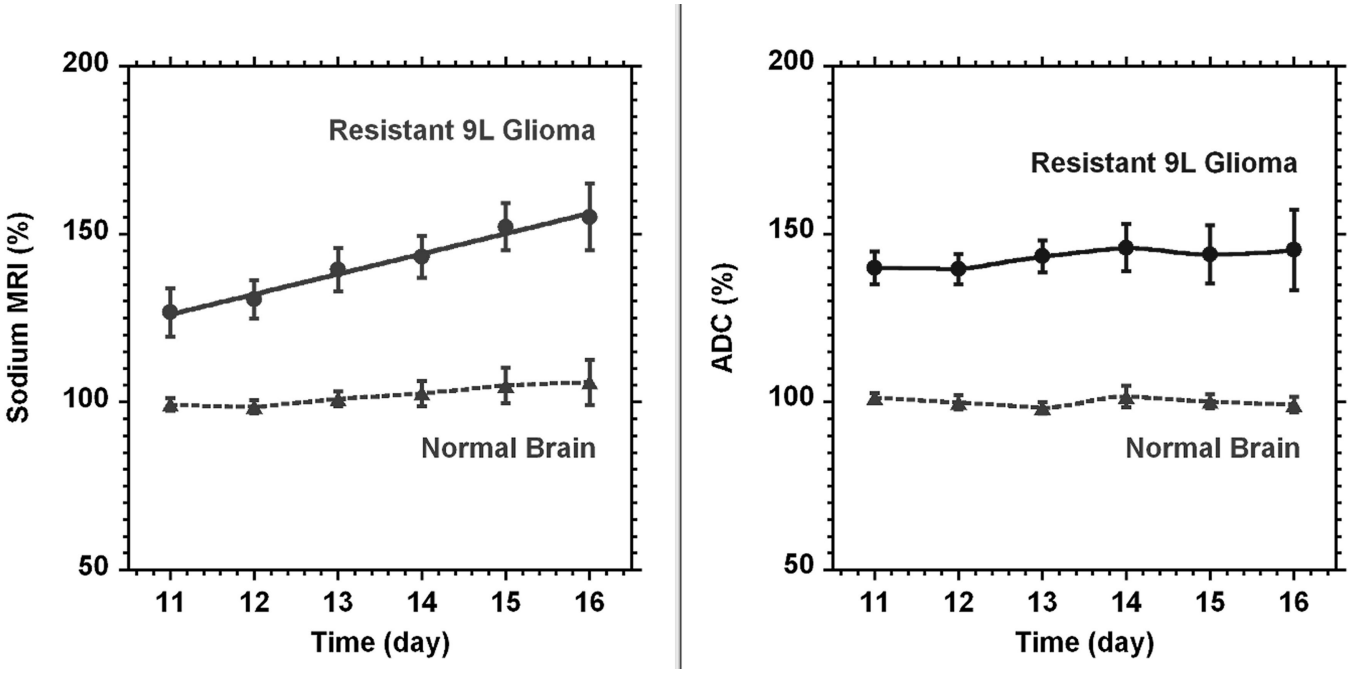

Fig. 5.

The time courses of sodium concentration (left) and diffusion (right) in rat glioma (●, n = 5) created from the resistant 9L cell line. The time scale on the figure was given from tumor implantation. Sodium and diffusion in the tumor are presented as percent relative to the normal contra-lateral part of the brain (▲). The reference (100%) was the average of all sodium or diffusion data through the time course. All points are given as mean ± SD. Linear fit of sodium and diffusion data for the tumor gave a sodium increase in time at a rate of 5.8 ± 0.8% (SD) per day and almost no change in diffusion (1.2 ± 0.8% (SD) per day). Curves for normal brain and diffusion in glioma were created by smooth function.

NIH-PA Author Manuscript
NIH-PA Author Manuscript
NIH-PA Author Manuscript

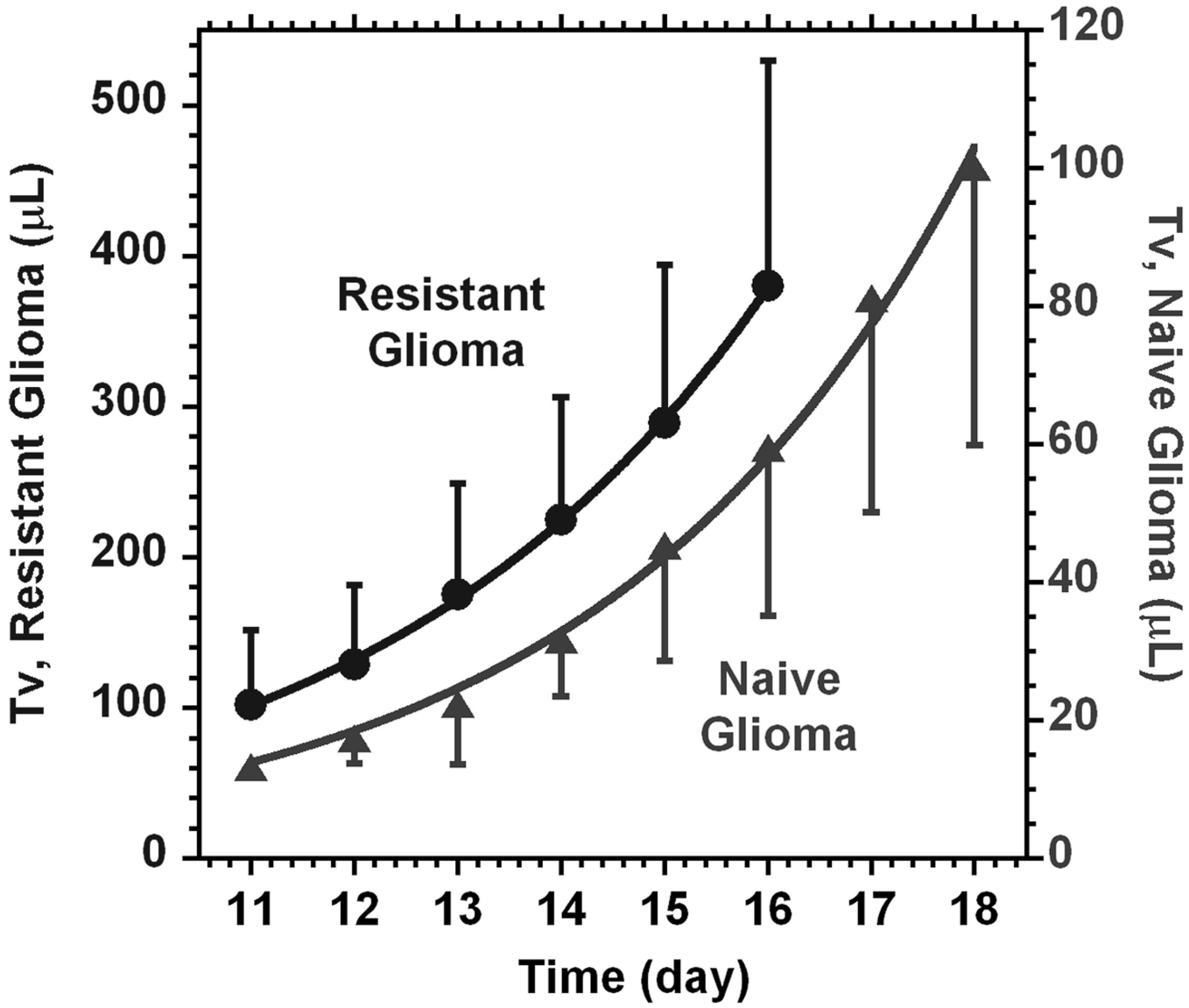

Fig. 6.

The time courses of tumor volume changes from day 11 after surgery for naïve (▲) and resistant (●) 9L cell lines. Curve lines represent the results of fitting to a model function ($Tv = a1*(2)^{time/a2}$). From the fit, the tumor doubling time $a2$ for naïve cells is 2.6 ± 0.1 (SD) days and the corresponding doubling time for the resistant cell line is 2.4 ± 0.2 (SD) days.

NIH-PA Author Manuscript
NIH-PA Author Manuscript
NIH-PA Author Manuscript

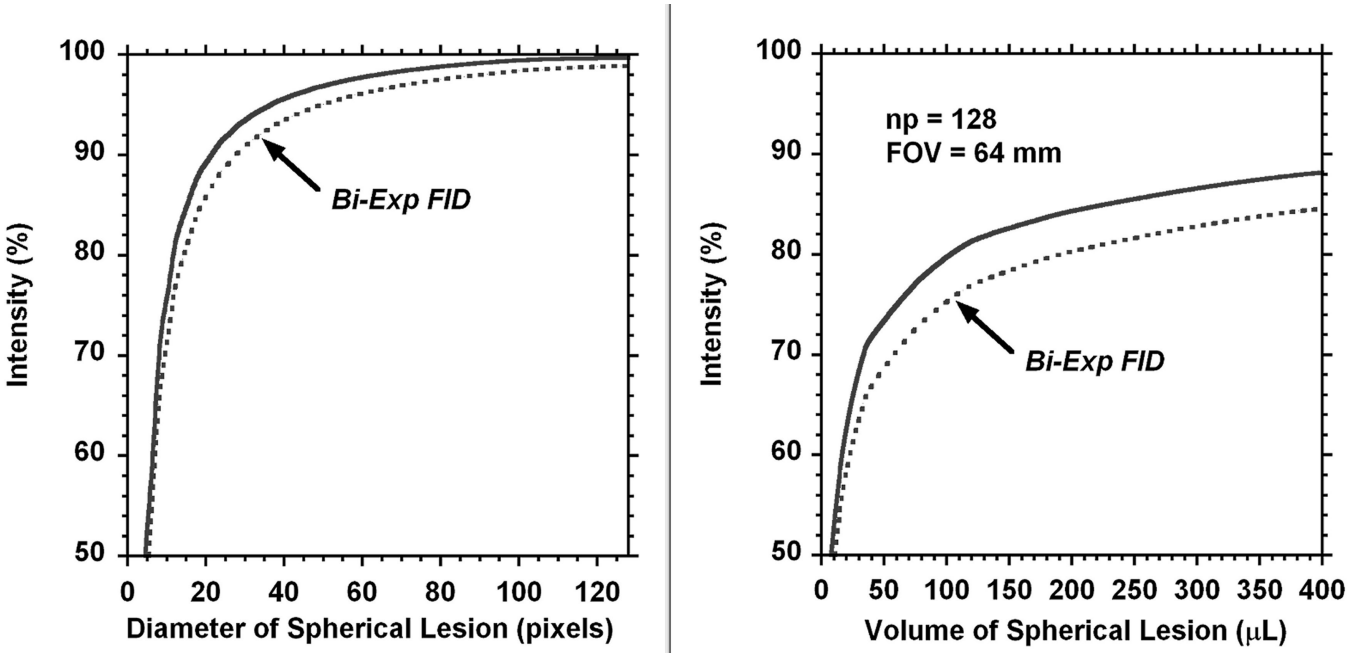

Fig. 7.

3D model of the partial volume effect in MRI. Lesion had spherical size with a diameter presented by pixel number (x-axis). The average intensity of each voxel (y-axis) in the lesion is given relative to the lesion reference with the size of FOV and covered by matrix of 128×128×128 (left part). The right side represents the PV effect for the range of tumor volumes detected in the present experiments. Both parts of the figure represent PV effect for the MRI intensity of lesion relative to the surrounding area. The dotted lines present a possible additional contribution which may occur due to the bi-exponential decay of the FID. The shape of the bi-exponential function is described in the text.

NIH-PA Author Manuscript
NIH-PA Author Manuscript
NIH-PA Author Manuscript

Table 1

Exponential non-linear fit ($y = m1 + m2*\exp(-c / m3)$) of 9L cell survival during cultivation in media with different concentrations of BCNU.

	***m*1 (%)**	**SD (*m*1)**	***m*2 (%)**	**SD (*m*2)**	***m*3 (μM)**	**SD (*m*3)**	**R^2***
Naïve 9L cell type (n = 6)	17.2	1.6	82.6	2.7	19.1	1.6	0.9991
Resistant 9L cell type (n = 3)	34.7	2.0	65.0	3.3	31.2	4.1	0.998

*R^2 - regression coefficient representing a quality of the fit.